
A Differential Geometric Approach to Classification

Qinxun Bai

Department of Computer Science
Boston University
qinxun@cs.bu.edu

Steven Rosenberg

Department of Mathematics and Statistics
Boston University
sr@math.bu.edu

Stan Sclaroff

Department of Computer Science
Boston University
sclaroff@cs.bu.edu

Zheng Wu

The Mathworks. Inc
wuzheng@bu.edu

Abstract

We use differential geometry techniques to estimate the class probability $P(y = \ell | \mathbf{x})$ for learning both binary and multiclass plug-in classifiers. We propose a geometric regularization technique to find the optimal submanifold corresponding to the estimator of $P(y = \ell | \mathbf{x})$. The regularization term measures the volume of this submanifold, based on the intuition that overfitting produces fast oscillations and hence large volume of the estimator. We use gradient flow methods to move from an initial estimator towards a minimizer of a penalty function that penalizes both the deviation of the submanifold from the training data and large volume. We establish Bayes consistency for our algorithm under mild initialization assumptions. In experiments for both binary and multiclass classification, our implementation compares favorably to several widely used classification methods.

1 Introduction

We study the classification problem in the probabilistic setting. Given a sample space \mathcal{X} , a label space \mathcal{Y} , and a finite training set of labeled samples $\mathcal{T}_m = \{(\mathbf{x}_i, y_i)\}_{i=1}^m$, where each training sample is generated i.i.d. from distribution P over $\mathcal{X} \times \mathcal{Y}$, our goal is to find a $h_{\mathcal{T}_m} : \mathcal{X} \rightarrow \mathcal{Y}$ such that for any new sample $\mathbf{x} \in \mathcal{X}$, $h_{\mathcal{T}_m}$ predicts its label $\hat{y} = h_{\mathcal{T}_m}(\mathbf{x})$. For general (binary or multiclass) classification where $\mathcal{Y} = \{1, \dots, L\}$, the optimal generalization risk (Bayes risk) is achieved by the classifier $h^*(\mathbf{x}) = \operatorname{argmax}_{\ell \in \mathcal{Y}} \{\eta^\ell(\mathbf{x})\}$, where $\boldsymbol{\eta} = (\eta^1, \dots, \eta^L)$ with $\eta^\ell : \mathcal{X} \rightarrow [0, 1]$ being the ℓ^{th} class probability, i.e. $\eta^\ell(\mathbf{x}) = P(y = \ell | \mathbf{x})$. Our method follows the plug-in classification scheme [3], i.e. find a nonparametric estimator $\mathbf{f} : \mathcal{X} \rightarrow \Delta^{L-1}$, where Δ^{L-1} is the standard $(L-1)$ -simplex in \mathbb{R}^L , $\mathbf{f} = (f^1, \dots, f^L)$ with $\sum_{\ell=1}^L f^\ell = 1$, and $f^\ell : \mathcal{X} \rightarrow [0, 1]$ as an estimator of η^ℓ , and then “plug-in” \mathbf{f} to get the plug-in classifier $h_{\mathbf{f}}(\mathbf{x}) = \operatorname{argmax}_{\ell \in \mathcal{Y}} \{f^\ell(\mathbf{x})\}$.

In learning \mathbf{f} we seek a balance between a perfect description of the training data and the potential for generalization. Regularized ERM (empirical risk minimization) [18, 17] is a commonly used framework for attaining this balance. However, we feel there is important local geometric information overlooked by ERM-based regularization methods, which usually constrain the complexity of the function class via a global norm. In many real world problems, if the feature space is meaningful, then all samples within a small enough neighborhood of a training sample should have class probability $\boldsymbol{\eta}(\mathbf{x})$ similar to the training sample. For instance, a small enough perturbation of RGB values at some pixels of a human face image should not change the identity of this image during face recognition. Thus, overfitting is related to rapid oscillations of the estimator \mathbf{f} of $\boldsymbol{\eta}$. From a geometric perspective, if we regard $\{(\mathbf{x}, \mathbf{f}(\mathbf{x}))\}$, the functional graph of \mathbf{f} , as a submanifold in $\mathcal{X} \times \Delta^{L-1}$, these oscillations can be measured by the total curvature or the volume of this submanifold.

In our approach, the learning process is formulated as a submanifold fitting problem that is solved by a geometric flow method. In particular, our approach finds a submanifold by iteratively fitting the training samples in a curvature or volume decreasing manner without any *a priori* assumptions on the geometry of the submanifold in $\mathcal{X} \times \Delta^{L-1}$. We use gradient flow methods to find an optimal direction, i.e. at each step we find the vector field pointing in the optimal direction to move \mathbf{f} . We show that under some mild assumptions on initialization, our algorithm is Bayes consistent. In experiments, our formulation compares favorably to widely used binary and multiclass classification methods on datasets from the UCI repository.

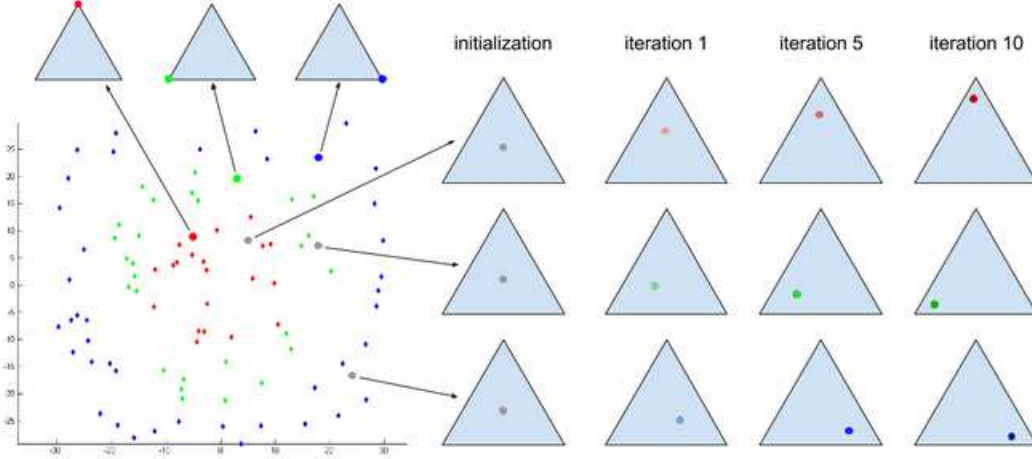


Figure 1: Example of three-class learning, i.e., $L = 3$, where the input space \mathcal{X} is $2d$. Training samples of the three classes are marked with red, green and blue dots respectively. The class label for each training sample corresponds to a vertex of the simplex Δ^{L-1} . We also plot the function values $\mathbf{f}(\mathbf{x})$ at three unlabeled points (grey dots in the plane) by showing their positions inside the standard simplex Δ^2 as our gradient flow method iterates during training.

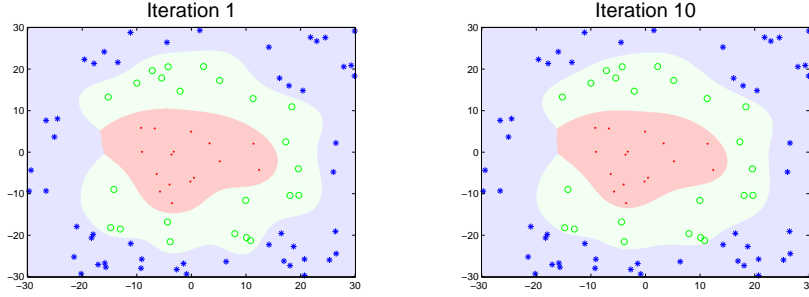


Figure 2: Decision boundaries estimated for the example in Figure 1 at iterations 1 and 10.

Figure 1 shows an example of learning using our approach, for a synthetic three-class problem. In this simple example, the domain \mathcal{X} is $2d$. The function value at each point $\mathbf{f}(\mathbf{x})$ evolves inside the simplex Δ^2 during training. In this example, $\mathbf{f}(\mathbf{x})$ is initialized to $(\frac{1}{3}, \frac{1}{3}, \frac{1}{3})$ everywhere. With each iteration during training, a gradient flow method is used to move $\mathbf{f}(\mathbf{x})$ towards a minimizer of a penalty function that penalizes both the deviation of the submanifold from the training data and large volume. The estimated class boundaries at iterations 1 and 10 are shown in Figure 2. Additional examples are given in Appendix D.

In summary, our contributions are:

1. We propose a unified geometric setup for binary and multiclass classification, which estimates the class probability $\boldsymbol{\eta}$ by fitting a submanifold corresponding to the estimator of $\boldsymbol{\eta}$.
2. We propose a geometric regularization term using the volume of the corresponding submanifold as a remedy to overfitting for the estimator of $\boldsymbol{\eta}$.
3. Our gradient flow method is Bayes consistent and produces strong numerical results.

2 Related Work

As discussed above, we introduce geometric methods to simultaneously treat binary and multiclass classification schemes. To the best of our knowledge, this framework does not exist in the current machine learning literature.

Our minimization formula can be viewed as a “hybrid” plug-in/empirical loss minimization (ERM) scheme [3], in the sense that the data term is most closely related to the k-nearest neighbor plug-in classifier [8, 9], while the overall loss minimization setup is similar to the regularized ERM. There is work using geometric regularization terms to measure the “smoothness” of the decision boundary [7, 21, 13]; Closely related work involving geometric regularization terms includes [5] and [21]. In both papers, the geometric terms are supported on submanifolds of the domain \mathcal{X} , the support of the training data in [5] and the decision boundary in [19]. In contrast, our geometric terms are supported on $\text{gr}(\mathbf{f})$ in $\mathcal{X} \times \Delta^{L-1}$, which is directly related to the class probability $\boldsymbol{\eta}$. In addition, these papers follow the standard regularized ERM scheme, while our hybrid scheme allows us to treat the multiclass and binary cases simultaneously.

Our training procedure for finding the optimal graph of a function is, in a general sense, also related to the manifold learning problem [20, 16, 4, 10, 22, 14]. The most closely related work is [10], which also seeks a flat submanifold of Euclidean space that contains a dataset. Again, there are key differences. Since the goal of [10] is dimensionality reduction, their manifold has high codimension, while our graph has codimension $L - 1$, which may be as low as 1. More importantly, we do not assume that the graph of our initial function is a flat (or volume minimizing) submanifold, and we instead flow towards a function whose graph is as flat (or volume minimizing) as possible. In this regard, our work is related to a large body of literature on gradient flow/Morse theory in finite and infinite dimensions, and on mean curvature flow.

3 The Differential Geometric Method

The submanifold of $\mathcal{X} \times \mathbb{R}^L$ associated with estimator $\mathbf{f} : \mathcal{X} \rightarrow \Delta^{L-1}$ is the graph (in the geometric sense) of \mathbf{f} : $\text{gr}(\mathbf{f}) = \{(\mathbf{x}, f^1(\mathbf{x}), \dots, f^L(\mathbf{x})) : \mathbf{x} \in \mathcal{X}\}$. Here $\Delta^{L-1} = \{(y^1, \dots, y^L) \in \mathbb{R}^L : y^\ell \geq 0, \sum_\ell y^\ell = 1\}$. For example, for $\boldsymbol{\eta}(\mathbf{x})$, we have $\mathcal{X} \subseteq \mathbb{R}^N, \mathcal{Y} = \{1, \dots, L\}, \mathcal{X} \times \Delta^{L-1} \subset \mathbb{R}^{N+L}$ with coordinates $(\mathbf{x}, \mathbf{z}) = (x^1, \dots, x^N, z^1, \dots, z^L)$, where $\mathbf{x} \in \mathcal{X}$ and $\mathbf{z} = (\eta^1(\mathbf{x}), \dots, \eta^L(\mathbf{x})) \in \Delta^{L-1}$. Each training point $(\mathbf{x}_i, y_i = \ell)$ maps to $(\mathbf{x}_i, \mathbf{z}_i) = (\mathbf{x}_i, 0, \dots, 1, \dots, 0)$ with the 1 in the ℓ slot; \mathbf{z}_i is the vertex of Δ^{L-1} corresponding to $P(y = y_i | \mathbf{x}) = 1$.

We want \mathbf{f} to approach the mapped training points while remaining as flat as possible, so we impose a penalty on the graph of \mathbf{f} consisting of a data term \mathcal{P}_D and a geometric regularization term \mathcal{P}_G . For \mathcal{P}_D , we define a distance penalty on $\text{gr}(\mathbf{f})$ that is an L^2 measure of the distance in \mathbb{R}^L from the \mathbf{z} component of a graph point to the averaged \mathbf{z} component of its nearest training points. For \mathcal{P}_G , we would ideally consider an L^2 measure of the curvature of $\text{gr}(\mathbf{f})$, as the vanishing of this term gives optimal (i.e., local distortion free) diffeomorphisms from $\text{gr}(\mathbf{f})$ to \mathbb{R}^N . For computational reasons, we measure the graph’s volume, $\mathcal{P}_G(\mathbf{f}) = \int_{\text{gr}(\mathbf{f})} \text{dvol}$, where dvol is the induced volume from the Lebesgue measure on \mathbb{R}^{N+L} , as volume minimizing maps intuitively are not rapidly oscillating. It is important to note that any relative scaling between the domain \mathcal{X} and the range Δ^{L-1} will not affect the estimate of the class probability $\boldsymbol{\eta}$, as scaling will distort $\text{gr}(\mathbf{f})$ but will not change the critical function estimating $\boldsymbol{\eta}$.

More precisely, we consider the following penalty function, where λ is the trade-off parameter:

$$\mathcal{P} = \mathcal{P}_D + \lambda \mathcal{P}_G : \mathcal{M} = \text{Maps}(\mathcal{X}, \Delta^{L-1}) \rightarrow \mathbb{R}$$

on the set \mathcal{M} of smooth functions from \mathcal{X} to Δ^{L-1} . Finding $\text{argmin } \mathcal{P}$ directly is too difficult, so we use gradient flow methods. For the moment, we will replace \mathcal{M} with a finite dimensional Riemannian manifold M . If \mathcal{P} is smooth, it has a differential $d\mathcal{P}_{\mathbf{f}} : T_{\mathbf{f}}M \rightarrow \mathbb{R}$ for each $\mathbf{f} \in M$, where $T_{\mathbf{f}}M$ is the tangent space to M at \mathbf{f} . Since $d\mathcal{P}_{\mathbf{f}}$ is a linear functional on $T_{\mathbf{f}}M$, there is a unique tangent vector, denoted $\nabla \mathcal{P}_{\mathbf{f}}$, such that $d\mathcal{P}_{\mathbf{f}}(\mathbf{v}) = \langle \mathbf{v}, \nabla \mathcal{P}_{\mathbf{f}} \rangle$ for all $\mathbf{v} \in T_{\mathbf{f}}M$. $\nabla \mathcal{P}_{\mathbf{f}}$ points in the direction of maximal increase of \mathcal{P} at \mathbf{f} . Thus, the solution of the negative gradient flow $d\mathbf{f}_t/dt = -\nabla \mathcal{P}_{\mathbf{f}_t}$ is a flow line of steepest descent starting at an initial \mathbf{f}_0 . For a dense open set of initial points, flow lines approach a local minimum of \mathcal{P} at $t \rightarrow \infty$.

In our setup, we want to find the (or a) best estimator $\mathbf{f} : \mathcal{X} \rightarrow \Delta^{L-1}$ of $\boldsymbol{\eta}$ on a compact set $\mathcal{X} \subset \mathbb{R}^N$ given a set of training data $\mathcal{T}_m = \{(\mathbf{x}_i, y_i)\}_{i=1}^m$. We think of \mathcal{X} as large enough so that the training data actually is sampled well inside \mathcal{X} . This allows us to treat \mathcal{X} as a closed manifold in our gradient calculations, so that boundary effects can be ignored.

We implement gradient flow methods on the infinite dimensional manifold \mathcal{M} . To do so, we have to understand both the topology and the Riemannian geometry of \mathcal{M} . For the topology, we put the Fréchet topology on $\mathcal{M}' = \text{Maps}(\mathcal{X}, \mathbb{R}^L)$, the set of smooth maps from \mathcal{X} to \mathbb{R}^L , and take the induced topology on \mathcal{M} . Intuitively speaking, two functions in \mathcal{M} are close if the functions and all their partial derivatives are pointwise close.

\mathcal{M} is an open Fréchet submanifold with boundary inside the vector space \mathcal{M}' , so as with an open set in Euclidean space, we can canonically identify $T_{\mathbf{f}}\mathcal{M}$ with \mathcal{M}' . For the Riemannian metric, we take the L^2 metric on each tangent space $T_{\mathbf{f}}\mathcal{M}$: $\langle \phi_1, \phi_2 \rangle := \int_{\mathcal{X}} \phi_1(\mathbf{x})\phi_2(\mathbf{x})\text{dvol}_{\mathbf{x}}$, with $\phi_i \in \mathcal{M}'$ and $\text{dvol}_{\mathbf{x}}$ being the volume form of the induced Riemannian metric on the graph of \mathbf{f} . (Strictly speaking, the volume form is pulled back to \mathcal{X} by \mathbf{f} , usually denoted $\mathbf{f}^*\text{dvol}$.)

The differential $d\mathcal{P}_{\mathbf{f}}$ is linear as above, and by a direct calculation, there is a unique tangent vector $\nabla\mathcal{P}_{\mathbf{f}} \in T_{\mathbf{f}}\mathcal{M}$ such that $d\mathcal{P}_{\mathbf{f}}(\phi) = \langle \nabla\mathcal{P}_{\mathbf{f}}, \phi \rangle$ for all $\phi \in T_{\mathbf{f}}\mathcal{M}$. Thus, we can construct the gradient flow equation. However, unlike the case of finite dimensions, the existence of flow lines is not automatic. Assuming the existence of flow lines, a generic initial point flows to a local minimum of \mathcal{P} . In any case, our numerical approximation in §5 mimicking gradient flow is well defined.

We always choose the initial function \mathbf{f}_0 to be the “neutral” choice $\mathbf{f}_0(\mathbf{x}) \equiv (\frac{1}{L}, \dots, \frac{1}{L})$ which reasonably assigns equal conditional probability to all classes. This choice works well in practice.

3.1 The distance penalty \mathcal{P}_D

Since \mathcal{P}_D measures the deviation of $\text{gr}(\mathbf{f})$ from the mapped training points, a natural geometric distance penalty term is an L^2 distance in \mathbb{R}^L from $\mathbf{f}(\mathbf{x})$ to the averaged z component of the k -nearest training points:

$$\mathcal{P}_D(\mathbf{f}) = R_{D, \mathcal{T}_m, k}(\mathbf{f}) = \int_{\mathcal{X}} d^2 \left(\mathbf{f}(\mathbf{x}), \frac{1}{k} \sum_{i=1}^k \tilde{\mathbf{z}}_i \right) d\mathbf{x}, \quad (1)$$

where d is the Euclidean distance in \mathbb{R}^L , $\tilde{\mathbf{z}}_i$ is the vector of the last L components of $(\tilde{\mathbf{x}}_i, \tilde{\mathbf{z}}_i) = (\tilde{\mathbf{x}}_i^1, \dots, \tilde{\mathbf{x}}_i^N, \tilde{\mathbf{z}}_i^1, \dots, \tilde{\mathbf{z}}_i^L)$, with $\tilde{\mathbf{x}}_i$ the i^{th} nearest neighbor of \mathbf{x} in \mathcal{T}_m , and $d\mathbf{x}$ is the Lebesgue measure. The gradient vector field is

$$\nabla(R_{D, \mathcal{T}_m, k})_{\mathbf{f}}(\mathbf{x}, \mathbf{f}(\mathbf{x})) = \frac{2}{k} \sum_{i=1}^k (\mathbf{f}(\mathbf{x}) - \tilde{\mathbf{z}}_i).$$

However, $\nabla(R_{D, \mathcal{T}_m, k})_{\mathbf{f}}$ is discontinuous on the set \mathcal{D} of points \mathbf{x} such that \mathbf{x} has equidistant training points among its k nearest neighbors. \mathcal{D} is the union of $(N-1)$ -dimensional hyperplanes in \mathcal{X} , so \mathcal{D} has measure zero. Such points will necessarily exist unless the last L components of the mapped training points are all 1 or all 0. To rectify this, we can smooth out $\nabla(R_{D, \mathcal{T}_m, k})_{\mathbf{f}}$ to a vector field

$$V_{D, \mathbf{f}, \phi} = \frac{2\phi(\mathbf{x})}{k} \sum_{i=1}^k (\mathbf{f}(\mathbf{x}) - \tilde{\mathbf{z}}_i). \quad (2)$$

Here $\phi(\mathbf{x})$ is a smooth damping function close to the singular function $\delta_{\mathcal{D}}$, which has $\delta_{\mathcal{D}}(\mathbf{x}) = 0$ for $\mathbf{x} \in \mathcal{D}$ and $\delta_{\mathcal{D}}(\mathbf{x}) = 1$ for $\mathbf{x} \notin \mathcal{D}$. Outside any open neighborhood of \mathcal{D} , $\nabla R_{D, \mathcal{T}_m, k} = V_{D, \mathbf{f}, \phi}$ for ϕ close enough to $\delta_{\mathcal{D}}$. $V_{D, \mathbf{f}, \phi}$ is no longer a gradient vector field, but this does not affect the theory in §4 or the computations in §5.

3.2 The geometric penalty \mathcal{P}_G

As discussed in §1, we wish to penalize graphs for excessive curvature. The most informative measure of intrinsic curvature is given by the L^2 norm of the Riemann curvature tensor: $\int_{\mathcal{X}} |\mathcal{R}_{\mathbf{f}}|^2 \text{dvol}$. However, the curvature tensor is complicated (see Appendix A), and the corresponding gradient

vector field is even more complicated and inefficient in practice. As a result, we use the following simpler function, which measures the volume of the $\text{gr}(\mathbf{f})$:

$$\mathcal{P}_G(\mathbf{f}) = \int_{\text{gr}(\mathbf{f})} \text{dvol}, \quad (3)$$

It is standard that $\nabla \mathcal{P}_G = -\text{Tr } \Pi \in \mathbb{R}^{N+L}$ on the space of all embeddings of \mathcal{X} in \mathbb{R}^{N+L} (see Appendix A). If we restrict to the submanifold of graphs of $\mathbf{f} \in \mathcal{M}'$, it is easy to calculate that the gradient of geometric penalty (3) is

$$V_{G,\mathbf{f}} \stackrel{\text{def}}{=} -\text{Tr } \Pi^L, \quad (4)$$

where $\text{Tr } \Pi^L$ denotes the last L components of $\text{Tr } \Pi$.

There is an explicit formula for the volume penalty gradient vector field for the multiclass case.

Theorem 1. For $\mathbf{f} : \mathbb{R}^N \rightarrow \mathbb{R}^L$, $\text{Tr } \Pi^L$ for $\text{gr}(\mathbf{f})$ is given by

$$\text{Tr } \Pi^L = (g^{-1})^{ij} \left(f_{ji}^1 - (g^{-1})^{rs} f_{rs}^a f_i^a f_j^1, \dots, f_{ji}^L - (g^{-1})^{rs} f_{rs}^a f_i^a f_j^L \right), \quad (5)$$

where f_i^a, f_{ij}^a denote partial derivatives of f^a , and $g = (g_{ij})$ with $g_{ij} = \delta_{ij} + f_i^a f_j^a$.

We use summation convention on repeated indices. The proof is in Appendix B.

3.3 Gradient method summary

For the penalty function $\mathcal{P} = \mathcal{P}_D + \lambda \mathcal{P}_G$, we have computed the gradient vector field $V_{tot,\lambda,m,\mathbf{f},\phi}$ of \mathcal{P} , which by (2) and (4) is

$$\begin{aligned} V_{tot,\lambda,m,\mathbf{f},\phi} &= \nabla \mathcal{P}_f = V_{D,\mathbf{f},\phi} + \lambda V_{G,\mathbf{f}} \\ &= \frac{2\phi(\mathbf{x})}{k} \sum_{i=1}^k (\mathbf{f}(\mathbf{x}) - \tilde{\mathbf{z}}_i) - \lambda \text{Tr } \Pi^L. \end{aligned} \quad (6)$$

Starting from $\mathbf{f}_0(\mathbf{x}) \equiv (\frac{1}{L}, \dots, \frac{1}{L})$, the gradient flow line, i.e., the solution of $\frac{d\mathbf{f}_t}{dt} = -\nabla \mathcal{P}_{\mathbf{f}_t}$, should flow towards a local minimum of \mathcal{P} .

4 Consistency Analysis

For a training set \mathcal{T}_m , we let $\mathbf{f}_{\mathcal{T}_m} = (f_{\mathcal{T}_m}^1, \dots, f_{\mathcal{T}_m}^L)$ be the class probability estimator given by our approach. We denote the generalization risk of the corresponding plug-in classifier $h_{\mathbf{f}_{\mathcal{T}_m}}$ by $R_P(\mathbf{f}_{\mathcal{T}_m}) = \mathbb{E}_P[\mathbb{1}_{h_{\mathbf{f}_{\mathcal{T}_m}}(\mathbf{x}) \neq y}]$. The Bayes risk is defined by $R_P^* = \inf_{h:\mathcal{X} \rightarrow \mathcal{Y}} R_P(h) = \mathbb{E}_P[\mathbb{1}_{h_\eta(\mathbf{x}) \neq y}]$.

Our algorithm is Bayes consistent if $\lim_{m \rightarrow \infty} R_P(\mathbf{f}_{\mathcal{T}_m}) = R_P^*$ holds in probability for all distributions P on $\mathcal{X} \times \mathcal{Y}$. Usually, gradient flow methods are applied to a convex functional, so that a flow line approaches the unique global minimum. If the domain of the functional is an infinite dimensional manifold of (e.g. smooth) functions, we always assume that flow lines exist and that the actual minimum exists in this manifold.

Because our functionals are not convex, and because we are strictly speaking not working with gradient vector fields, we can only hope to prove Bayes consistency for the set of initial estimators in the stable manifold of a stable fixed point (or sink) of the vector field [12]. Recall that a stable fixed point \mathbf{f}_0 has a maximal open neighborhood, the stable manifold $\mathcal{S}_{\mathbf{f}_0}$, on which flow lines tend towards \mathbf{f}_0 . For the manifold \mathcal{M} , the stable manifold for a stable critical point of the vector field $V_{tot,\lambda,m,\mathbf{f},\phi}$ is infinite dimensional.

The proof of Bayes consistency for multiclass (including binary) classification follows these steps:

Step 1: $\lim_{\lambda \rightarrow 0} R_{D,P,\lambda}^* = 0$.

Step 2: $\lim_{n \rightarrow \infty} R_{D,P}(\mathbf{f}_n) = 0 \Rightarrow \lim_{n \rightarrow \infty} R_P(\mathbf{f}_n) = R_P^*$.

Step 3: For all $\mathbf{f} \in \mathcal{M} = \text{Maps}(\mathcal{X}, \Delta^{L-1})$, $|R_{D, \mathcal{T}_m}(\mathbf{f}) - R_{D, P}(\mathbf{f})| \xrightarrow{m \rightarrow \infty} 0$ in probability.

For the notation see Appendix A. $R_{D, P, \lambda}^*$ is the minimum of the regularized D risk $R_{D, P, \lambda}(\mathbf{f})$ for \mathbf{f} : $R_{D, P, \lambda}(\mathbf{f}) = R_{D, P}(\mathbf{f}) + \lambda \mathcal{P}_G(\mathbf{f})$, with $R_{D, P}(\mathbf{f}) = \int_{\mathcal{X}} d^2(\mathbf{f}(\mathbf{x}), \boldsymbol{\eta}(\mathbf{x})) d\mathbf{x}$ the D -risk. Also, $R_{D, \mathcal{T}_m, \lambda}(\mathbf{f}) = R_{D, \mathcal{T}_m}(\mathbf{f}) + \lambda \mathcal{P}_G(\mathbf{f})$, with $R_{D, \mathcal{T}_m}(\mathbf{f}) = \int_{\mathcal{X}} d^2\left(\mathbf{f}(\mathbf{x}), \frac{1}{k} \sum_{i=1}^k \tilde{\mathbf{z}}_i\right) d\mathbf{x}$ the empirical D -risk. For proofs, see Appendix C.

Theorem 2 (Bayes Consistency). *Let m be the size of the training data set. Let $\mathbf{f}_{1, \lambda, m} \in \mathcal{S}_{\mathbf{f}_{D, \mathcal{T}_m, \lambda}}$, the stable manifold for the global minimum $\mathbf{f}_{D, \mathcal{T}_m, \lambda}$ of $R_{D, \mathcal{T}_m, \lambda}$, and let $\mathbf{f}_{n, \lambda, m, \phi}$ be a sequence of functions on the flow line of $V_{tot, \lambda, m, \mathbf{f}, \phi}$ starting with $\mathbf{f}_{1, \lambda, m}$ with the flow time $t_n \rightarrow \infty$ as $n \rightarrow \infty$. Then $R_P(\mathbf{f}_{n, \lambda, m, \phi}) \xrightarrow[\lambda \rightarrow 0, \phi \rightarrow \delta_{\mathcal{D}}]{m, n \rightarrow \infty} R_P^*$ in probability for all distributions P on $\mathcal{X} \times \mathcal{Y}$, if $k/m \rightarrow 0$ as $m \rightarrow \infty$.*

Proof. In the notation of Appendix A, if $\mathbf{f}_{D, \mathcal{T}_m, \lambda}$ is a global minimum for $R_{D, \mathcal{T}_m, \lambda}$, then outside of \mathcal{D} , $\mathbf{f}_{D, \mathcal{T}_m, \lambda}$ is the limit of critical points for the negative flow of $V_{tot, \lambda, m, \mathbf{f}, \phi}$ as $\phi \rightarrow \delta_{\mathcal{D}}$. To see this, fix an ϵ_i neighborhood \mathcal{D}_{ϵ_i} of \mathcal{D} . For a sequence $\phi_j \rightarrow \delta_{\mathcal{D}}$, $V_{tot, \lambda, m, \mathbf{f}, \phi_j}$ is independent of $j \geq j(\epsilon_i)$ on $\mathcal{X} \setminus \mathcal{D}_{\epsilon_i}$, so we find a function \mathbf{f}_i , a critical point of $V_{tot, \lambda, m, \mathbf{f}, \phi_j(\epsilon_i)}$, equal to $\mathbf{f}_{D, \mathcal{T}_m, \lambda}$ on $\mathcal{X} \setminus \mathcal{D}_{\epsilon_i}$. Since any $\mathbf{x} \notin \mathcal{D}$ lies outside some \mathcal{D}_{ϵ_i} , the sequence \mathbf{f}_i converges at \mathbf{x} if we let $\epsilon_i \rightarrow 0$. Thus we can ignore the choice of ϕ in our proof, and drop ϕ from the notation.

For our algorithm, for fixed λ, m , we have as above $\lim_{n \rightarrow \infty} \mathbf{f}_{n, \lambda, m} = \mathbf{f}_{D, \mathcal{T}_m, \lambda}$, so

$$\lim_{n \rightarrow \infty} R_{D, \mathcal{T}_m, \lambda}(\mathbf{f}_{n, \lambda, m}) = R_{D, \mathcal{T}_m, \lambda}(\mathbf{f}_{D, \mathcal{T}_m, \lambda}),$$

for $\mathbf{f}_1 \in \mathcal{S}_{\mathbf{f}_{D, \mathcal{T}_m, \lambda}}$. By Step 2, it suffices to show $R_{D, P}(\mathbf{f}_{D, \mathcal{T}_m, \lambda}) \xrightarrow[\lambda \rightarrow 0]{m \rightarrow \infty} 0$. In probability, we have $\forall \delta > 0, \exists m > 0$ such that

$$\begin{aligned} R_{D, P}(\mathbf{f}_{D, \mathcal{T}_m, \lambda}) &\leq R_{D, P}(\mathbf{f}_{D, \mathcal{T}_m, \lambda}) + \lambda \mathcal{P}_G(\mathbf{f}_{D, \mathcal{T}_m, \lambda}) \leq R_{D, \mathcal{T}_m}(\mathbf{f}_{D, \mathcal{T}_m, \lambda}) + \lambda \mathcal{P}_G(\mathbf{f}_{D, \mathcal{T}_m, \lambda}) + \frac{\delta}{3} \quad (\text{Step 3}) \\ &= R_{D, \mathcal{T}_m, \lambda}(\mathbf{f}_{D, \mathcal{T}_m, \lambda}) + \frac{\delta}{3} \leq R_{D, \mathcal{T}_m, \lambda}(\mathbf{f}_{D, P, \lambda}) + \frac{\delta}{3} \quad (\text{minimality of } \mathbf{f}_{D, \mathcal{T}_m, \lambda}) \\ &= R_{D, \mathcal{T}_m}(\mathbf{f}_{D, P, \lambda}) + \lambda \mathcal{P}_G(\mathbf{f}_{D, P, \lambda}) + \frac{\delta}{3} \leq R_{D, P}(\mathbf{f}_{D, P, \lambda}) + \lambda \mathcal{P}_G(\mathbf{f}_{D, P, \lambda}) + \frac{2\delta}{3} \quad (\text{Step 3}) \\ &= R_{D, P, \lambda}(\mathbf{f}_{D, P, \lambda}) + \frac{2\delta}{3} = R_{D, P, \lambda}^* + \frac{2\delta}{3} \\ &\leq \delta, \quad (\text{Step 1}) \end{aligned}$$

for λ close to zero. Since $R_{D, P}(\mathbf{f}_{D, \mathcal{T}_m, \lambda}) \geq 0$, we are done. \square

5 Implementation

5.1 Parametric representation of \mathbf{f}

While the theory in §3 treats the domain of \mathbf{f} as a continuous space, for practical computations we adopt a parametric representation, as used in [15, 11] for level set functions. We choose to represent our nonparametric estimator \mathbf{f} by radial basis functions (RBFs),

$$\mathbf{f}(\mathbf{x}) = (f^1(\mathbf{x}), \dots, f^L(\mathbf{x})) = \left(\sum_{i=1}^m a_i^1 \varphi_i(\mathbf{x}), \dots, \sum_{i=1}^m a_i^L \varphi_i(\mathbf{x}) \right), \quad (7)$$

where $\varphi_i(\mathbf{x}) = e^{-\|\mathbf{x} - \mathbf{x}_i\|^2 / 2\sigma_i^2}$ is the RBF function centered at training sample \mathbf{x}_i , with kernel width parameter σ_i .

Estimating \mathbf{f} becomes an optimization problem for the $m \times L$ coefficient matrix $A = (a_i^\ell)$. For the $m \times m$ matrix $G = (G_{ij}) = (\varphi_j(\mathbf{x}_i))$, the following equation determines A :

$$[\mathbf{f}(\mathbf{x}_1), \dots, \mathbf{f}(\mathbf{x}_m)]^T = GA. \quad (8)$$

To plug this RBF representation into our gradient flow scheme, the total vector field given by (6) is evaluated at each sample point \mathbf{x}_i , and A is updated by

$$A \leftarrow A - \tau G^{-1} [V_{tot, \lambda, m, \mathbf{f}, \phi}(\mathbf{x}_1), \dots, V_{tot, \lambda, m, \mathbf{f}, \phi}(\mathbf{x}_m)]^T, \quad (9)$$

where τ is the step-size parameter.

The vector field is only evaluated at the sample points, which are also centers of the RBF functions, so it is reasonable to set $k = 1$ for the distance vector field given by (2). Thus there is no need for the damping function ϕ of (2). Since the RBF function is smooth and plays a role similar to the damping function, we need to specify a reasonable kernel width for the RBF functions that reflect the set \mathcal{D} discussed in §3.1. We adopt the p -nearest heuristic suggested by [6] with an extra constant c over all RBFs:

$$\sigma_i = \frac{c}{p} \left(\sum_{j=1}^p \|\mathbf{x}_i - \mathbf{x}_{j(i)}\|^2 \right)^{\frac{1}{2}}, \quad (10)$$

where $\mathbf{x}_{j(i)}$ is the j -th nearest neighbor to \mathbf{x}_i and we fix $p = 5$.

In summary, the total vector field for RBF representation is

$$V_{tot, \lambda, m, \mathbf{f}} = 2(\mathbf{f}(\mathbf{x}) - \tilde{\mathbf{z}}_1) - \lambda \text{Tr } \Pi^L, \quad (11)$$

and the final predictor learned by our method is given by

$$F(\mathbf{x}) = \text{argmax}\{f^\ell(\mathbf{x}), \ell \in \{1, 2, \dots, L\}\}. \quad (12)$$

A summary of the algorithm is given in Algorithm 1.

Algorithm 1 Geometric algorithm for classification

Input: training data $\mathcal{T}_m = \{(\mathbf{x}_i, y_i)\}_{i=1}^m$, constant c in (10), trade-off parameter λ , step-size τ
Initialize: $\mathbf{f}(\mathbf{x}_i) = (\frac{1}{L}, \dots, \frac{1}{L}) \forall i \in \{1, \dots, m\}$, solve A by (8)
for $t = 1$ **to** T **do**
 – Compute the gradient vector $V_{tot, \lambda, m, \mathbf{f}}(\mathbf{x}_i)$ for every data point according to (11).
 – Update the A by (9).
end for

5.2 Simplex constraint

Allowable estimators $\mathbf{f} : X \rightarrow \mathbb{R}^L$ actually take values in $\Delta^{L-1} \subset \mathbb{R}^L$ to ensure a proper estimate of $\boldsymbol{\eta}$. While this constraint is automatically satisfied for the flow of the distance gradient vector formula (2), it may fail for the flow of geometric gradient vector formula (4). There are two ways to enforce this constraint for the geometric gradient vector field. First, since our initial function \mathbf{f}_0 takes values at the center of Δ^{L-1} , we can orthogonally project the geometric gradient vector $V_{G, \mathbf{f}}$ to $V'_{G, \mathbf{f}}$ in the tangent space $Z = \{(y^1, \dots, y^L) \in \mathbb{R}^L : \sum_{\ell=1}^L y^\ell = 0\}$ of the simplex, and then scale $\tau V'_{G, \mathbf{f}}$ (τ is the stepsize) to ensure that the range of the new \mathbf{f}_1 lies in Δ^{L-1} . We then iterate. More simply, we can select $L - 1$ of the L components of $\mathbf{f}(\mathbf{x})$, call the new function $\mathbf{f}' : \mathcal{X} \rightarrow \mathbb{R}^{L-1}$, and compute the $(L - 1)$ -dimensional gradient vector $V_{g, \mathbf{f}'}$ following (4) and (5). The omitted component of the desired L -gradient vector is determined by $-\sum_{\ell=1}^{L-1} V_{g, \mathbf{f}'}^\ell$, by the definition of Z . Our implementation reported in next section follows this second approach, where we choose the $(L - 1)$ components of \mathbf{f} by omitting the component corresponding to the class with least number of training samples.

5.3 Experiments

We tested our classification method on four binary classification and four multiclass classification datasets. Our experimental setup follows [21], where the average test error is computed using ten-fold cross-validation. On each of the ten folds, the kernel-width constant c and tradeoff parameter λ are found using fivefold cross-validation, using the nine-tenths of the full dataset which is the

Table 1: Tenfold cross-validation error rate (percent) on four binary and four multiclass classification datasets from the UCI machine learning repository. (L, N) denote the number of classes and input feature dimensions respectively. We compare our method (Ours) with 10 methods reported in Table 1 of [21]: Naïve Bayes (NB), Bayes net (BN), k -nearest neighbor with inverse distance weighting (kNN), C4.4 decision tree (C4.4), C4.5 decision tree (C4.5), Naïve Bayes tree (NBT), SVM with polynomial kernel (SVM), Radial basis function network (RBN), Level learning set classifier [7] (LLS), Geometric level set classifier [21] (GLS). Top performance for each dataset is shown in bold.

| Dataset(L, N) | NB | BN | kNN | C4.4 | C4.5 | NBT | SVM | RBN | LLS | GLS | Ours |
|-------------------|-------|-------------|-------|-------|-------|--------------|--------------|-------|-------------|-------|--------------|
| Pima(2,8) | 23.69 | 25.64 | 27.86 | 27.33 | 26.17 | 25.64 | 22.66 | 24.60 | 29.94 | 25.94 | 25.93 |
| WDBC(2,30) | 7.02 | 4.92 | 3.68 | 7.20 | 6.85 | 7.21 | 2.28 | 5.79 | 6.50 | 4.40 | 1.75 |
| Liver(2,6) | 44.61 | 43.75 | 41.75 | 31.01 | 31.29 | 33.87 | 41.72 | 35.65 | 37.39 | 37.61 | 30.08 |
| Ionos.(2,34) | 17.38 | 10.54 | 17.38 | 8.54 | 8.54 | 10.27 | 11.40 | 7.38 | 13.11 | 13.67 | 4.27 |
| Wine(3,13) | 3.37 | 1.11 | 5.00 | 6.14 | 6.14 | 3.37 | 1.67 | 1.70 | 5.03 | 3.92 | 1.11 |
| Iris(3,4) | 4.00 | 7.33 | 4.67 | 4.00 | 4.00 | 6.00 | 4.00 | 4.67 | 3.33 | 6.00 | 4.00 |
| Glass(6,9) | 50.52 | 25.24 | 29.89 | 33.68 | 34.13 | 24.78 | 42.49 | 34.50 | 38.77 | 36.95 | 26.62 |
| Segm.(7,19) | 18.93 | 9.60 | 5.20 | 4.27 | 4.27 | 5.67 | 8.07 | 13.07 | 14.40 | 4.03 | 3.07 |

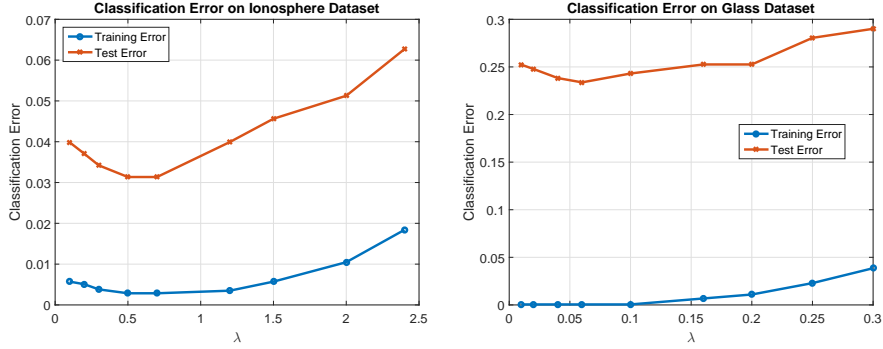


Figure 3: Tenfold cross-validation training error (blue) and testing error (red) for The Ionosphere and Glass datasets as a function of the trade-off parameter λ .

training data for that fold. We select c from the set of values $\{2, 4, 8, 16, 32, 64\}$ and λ from the set of values $\{1/1.5^4, 1/1.5^3, 1/1.5^2, 1/1.5, 1, 1.5\}$ that minimizes the fivefold cross-validation error. All dimensions of input sample points are normalized to a fixed range $[0, 10]$ throughout the experiments. (As noted above, scaling of the input space will not affect the estimate of $P(y = \ell | \mathbf{x})$.) The step-size $\tau = 0.1$ and iteration number $T = 5$ are fixed over all datasets.

Table 1 reports the results of this experiment. Our geometric method attains top performance on five out of the eight benchmarks, and overall is the strongest performer among all reported methods. We also study the classification error as a function of the tradeoff parameter λ , where c is fixed. Figure 3 shows the tenfold cross-validation training and testing error for the Ionosphere (binary) and Glass (multiclass) datasets. Similar behavior is observed for the other six datasets reported in Table 1.

To test our method on a challenging real-world application, we also conduct experiments on the Flickr Material Database (FMD) for image classification [1]. This dataset contains 10 categories of images with 100 images per category. We extract image features using the SIFT descriptor augmented by its feature coordinates, implemented by the VLFeat library [2]. With this descriptor, Bag-of-visual-words uses 4096 vector-quantized visual words, histogram square rooting, followed by L2 normalization. We compare our method with a baseline of one-vs-all linear SVM classifier using exactly the same 4096 dimensional feature. Our method achieves a correct classification rate of 48.8% while the baseline achieves 44.6%. We have also tested the one-vs-one scheme and the SVM with RBF kernel as alternative baselines, which achieves a correct classification rate of 46.4%. Our method is comparable with the state-of-the-art classification methods on this challenging real-world classification problem. Note that while there exist literature reporting better performance on this dataset, the feature used is more sophisticated, and thus, their results are not directly comparable.

6 Conclusion

We have proposed a geometric setup with a volume regularization term to uniformly solve binary and multiclass classification via gradient flow methods. Areas for future work include: studying the convergence rate of our algorithm, and parameterizations beyond RBFs.

References

- [1] FMD. <http://people.csail.mit.edu/celiu/CVPR2010/FMD/>. Accessed: 2015-06-01.
- [2] VLFeat. <http://www.vlfeat.org/applications/apps.html>. Accessed: 2015-06-01.
- [3] J.-Y. Audibert and A. Tsybakov. Fast learning rates for plug-in classifiers. *Annals of Statistics*, 35(2):608–633, 2007.
- [4] M. Belkin and P. Niyogi. Laplacian eigenmaps for dimensionality reduction and data representation. *Neural Computation*, 15(6):1373–1396, 2003.
- [5] M. Belkin, P. Niyogi, and V. Sindhwani. Manifold regularization: A geometric framework for learning from labeled and unlabeled examples. *Journal of Machine Learning Research*, 7:2399–2434, 2006.
- [6] N. Benoudjit and M. Verleysen. On the kernel widths in radial-basis function networks. *Neural Processing Letters*, 18(2):139–154, 2003.
- [7] X. Cai and A. Sowmya. Level learning set: A novel classifier based on active contour models. In *Proc. European Conf. on Machine Learning (ECML)*, pages 79–90. 2007.
- [8] T. Cover and P. Hart. Nearest neighbor pattern classification. *IEEE Trans. Information Theory*, 13(1):21–27, 1967.
- [9] L. Devroye, L. Györfi, and G. Lugosi. *A probabilistic theory of pattern recognition*. Springer, 1996.
- [10] D. Donoho and C. Grimes. Hessian eigenmaps: Locally linear embedding techniques for high-dimensional data. *Proceedings of the National Academy of Sciences*, 100(10):5591–5596, 2003.
- [11] A. Gelas, O. Bernard, D. Friboulet, and R. Prost. Compactly supported radial basis functions based collocation method for level-set evolution in image segmentation. *IEEE Trans. on Image Processing*, 16(7):1873–1887, 2007.
- [12] J. Guckenheimer and P. Worfolk. Dynamical systems: some computational problems. In *Bifurcations and periodic orbits of vector fields (Montreal, PQ, 1992)*, volume 408 of *NATO Adv. Sci. Inst. Ser. C Math. Phys. Sci.*, pages 241–277. Kluwer Acad. Publ., Dordrecht, 1993.
- [13] T. Lin, H. Xue, L. Wang, and H. Zha. Total variation and Euler’s elastica for supervised learning. *Proc. International Conf. on Machine Learning (ICML)*, 2012.
- [14] T. Lin and H. Zha. Riemannian manifold learning. *IEEE Trans. on Pattern Analysis and Machine Intelligence (PAMI)*, 30(5):796–809, 2008.
- [15] S. Osher and J. Sethian. Fronts propagating with curvature-dependent speed: algorithms based on hamilton-jacobi formulations. *Journal of Computational Physics*, 79(1):12–49, 1988.
- [16] S. Roweis and L. Saul. Nonlinear dimensionality reduction by locally linear embedding. *Science*, 290(5500):2323–2326, 2000.
- [17] B. Schölkopf and A. Smola. *Learning with kernels: Support vector machines, regularization, optimization, and beyond*. MIT press, 2002.
- [18] I. Steinwart. Consistency of support vector machines and other regularized kernel classifiers. *IEEE Trans. Information Theory*, 51(1):128–142, 2005.
- [19] C. Stone. Consistent nonparametric regression. *Annals of Statistics*, pages 595–620, 1977.
- [20] J. Tenenbaum, V. De Silva, and J. Langford. A global geometric framework for nonlinear dimensionality reduction. *Science*, 290(5500):2319–2323, 2000.

- [21] K. Varshney and A. Willsky. Classification using geometric level sets. *Journal of Machine Learning Research*, 11:491–516, 2010.
- [22] Z. Zhang and H. Zha. Principal manifolds and nonlinear dimensionality reduction via tangent space alignment. *SIAM Journal on Scientific Computing*, 26(1):313–338, 2005.

A Notation

Probability notation:

$$\begin{aligned}
h_{\mathbf{f}}(\mathbf{x}) = \operatorname{argmax}\{f^\ell(\mathbf{x}), \ell \in \mathcal{Y}\} & : \text{plug-in classifier of estimator } \mathbf{f} : \mathcal{X} \rightarrow \Delta^{L-1} \\
\mathbb{1}_{h_{\mathbf{f}}(\mathbf{x}) \neq y} & = \begin{cases} 1, & h_{\mathbf{f}}(\mathbf{x}) \neq y, \\ 0, & h_{\mathbf{f}}(\mathbf{x}) = y. \end{cases} \\
R_P(\mathbf{f}) = \mathbb{E}_P[\mathbb{1}_{h_{\mathbf{f}}(\mathbf{x}) \neq y}] & : \text{generalization risk for the estimator } \mathbf{f} \\
\boldsymbol{\eta}(\mathbf{x}) = (\eta^1(\mathbf{x}), \dots, \eta^L(\mathbf{x})) & : \text{class probability function: } \eta^\ell(\mathbf{x}) = P(y = \ell | \mathbf{x}) \\
R_P^* = R_P(\boldsymbol{\eta}) & : \text{Bayes risk} \\
(D\text{-risk for our } \mathcal{P}_D) R_{D,P}(\mathbf{f}) & = \int_{\mathcal{X}} d^2(\mathbf{f}(\mathbf{x}), \boldsymbol{\eta}(\mathbf{x})) d\mathbf{x} \\
(\text{empirical } D\text{-risk}) R_{D,\mathcal{T}_m}(\mathbf{f}) = R_{D,\mathcal{T}_m,k}(\mathbf{f}) & = \int_{\mathcal{X}} d^2\left(\mathbf{f}(\mathbf{x}), \frac{1}{k} \sum_{i=1}^k \tilde{\mathbf{z}}_i\right) d\mathbf{x} \\
& \text{where } \tilde{\mathbf{z}}_i \text{ is the vector of the last } L \text{ components of } \\
& (\tilde{\mathbf{x}}_i, \tilde{\mathbf{z}}_i), \text{ with } \tilde{\mathbf{x}}_i \text{ the } i^{\text{th}} \text{ nearest neighbor of } \mathbf{x} \text{ in } \mathcal{T}_m \\
(\text{volume penalty term}) \mathcal{P}_G(\mathbf{f}) & = \int_{\operatorname{gr}(\mathbf{f})} \operatorname{dvol} \\
R_{D,P,\lambda}(\mathbf{f}) = R_{D,P}(\mathbf{f}) + \lambda \mathcal{P}_G(\mathbf{f}) & : \text{regularized } D\text{-risk for estimator } \mathbf{f} \\
R_{D,\mathcal{T}_m,\lambda}(\mathbf{f}) = R_{D,\mathcal{T}_m}(\mathbf{f}) + \lambda \mathcal{P}_G(\mathbf{f}) & : \text{regularized empirical } D\text{-risk for estimator } \mathbf{f} \\
\mathbf{f}_{D,P,\lambda} & = \text{function attaining the global minimum for } R_{D,P,\lambda} \\
R_{D,P,\lambda}^* = R_{D,P,\lambda}(\mathbf{f}_{D,P,\lambda}) & : \text{minimum value for } R_{D,P,\lambda} \\
\mathbf{f}_{D,\mathcal{T}_m,\lambda} = \mathbf{f}_{D,\mathcal{T}_m,k,\lambda} & : \text{function attaining the global minimum for } R_{D,\mathcal{T}_m,\lambda}(\mathbf{f})
\end{aligned}$$

Note that we assume $\mathbf{f}_{D,P,\lambda}$ and $\mathbf{f}_{D,\mathcal{T}_m,\lambda}$ exist.

Geometry notation:

$$\begin{aligned}
\Delta^{L-1} & : \text{the standard } (L-1)\text{-simplex in } \mathbb{R}^L; \\
\Delta^{L-1} & = \{(y^1, \dots, y^L) : \sum_{\ell} y^\ell = 1, y^\ell \geq 0\} \\
\mathcal{M} & : \{f : \mathcal{X} \rightarrow \Delta^{L-1} : f \in C^\infty\} \\
\mathcal{M}' & : \{f : \mathcal{X} \rightarrow \mathbb{R}^L : f \in C^\infty\} \\
T_f \mathcal{M} & : \text{the tangent space to } \mathcal{M} \text{ at some } f \in \mathcal{M}; T_f \mathcal{M} \simeq \mathcal{M}' \\
\text{The graph of } f \in \mathcal{M} \text{ (or } \mathcal{M}') & : \operatorname{gr}(f) = \{(\mathbf{x}, f(\mathbf{x})) : \mathbf{x} \in \mathcal{X}\} \\
g_{ij} = \frac{\partial f}{\partial x^i} \frac{\partial f}{\partial x^j} & : \text{The Riemannian metric on the graph of } f \text{ induced from the} \\
& \text{standard dot product on } \mathbb{R}^{N+L} \\
(g^{ij}) & = g^{-1}, \text{ with } g = (g_{ij})_{i,j=1,\dots,N} \\
\operatorname{dvol}_{\mathbf{x}} = \operatorname{dvol}_{\operatorname{gr}(f)} & = \sqrt{\det(g)} dx^1 \dots dx^N, \text{ the volume element on } \operatorname{gr}(f) \\
\{e_i\}_{i=1}^N & : \text{a smoothly varying orthonormal basis of the tangent spaces} \\
& T_{(\mathbf{x}, f(\mathbf{x}))} \operatorname{gr}(f) \text{ of the graph of } f
\end{aligned}$$

Tr II : the trace of the second fundamental form of $\text{gr}(\mathbf{f})$;

$$\text{Tr II} \in \mathbb{R}^{N+L}; \text{Tr II} = \left(\sum_{i=1}^N D_{e_i} e_i \right)^\perp$$

with \perp the orthogonal projection to the subspace perpendicular to the tangent space of $\text{gr}(\mathbf{f})$

and $D_y w$ the directional derivative of w in the direction y

Tr II^L : the projection of Tr II onto the last L coordinates of \mathbb{R}^{N+L}

∇P : the gradient vector field of a function $P : A \rightarrow \mathbb{R}$ on a possibly infinite dimensional manifold A

$\mathcal{R} = \mathcal{R}_f$: the Riemannian curvature of the graph of f

\mathcal{R} is a four-tensor, with components $R_{sjkl} = g_{si} R^i_{jkl}$, with

$$R^i_{jkl} = \frac{\partial \Gamma^i_{jk}}{\partial x^l} - \frac{\partial \Gamma^i_{jl}}{\partial x^k} + \Gamma^t_{jk} \Gamma^i_{tl} - \Gamma^t_{jl} \Gamma^i_{tk}, \text{ with } \Gamma^i_{jk} = \frac{1}{2} g^{il} \left(\frac{\partial g_{kl}}{\partial x^j} + \frac{\partial g_{jl}}{\partial x^k} - \frac{\partial g_{jk}}{\partial x^l} \right),$$

with summation convention.

B Proof of Theorem 1

For $\mathbf{f} : \mathbb{R}^N \rightarrow \mathbb{R}^L$,

$$\{r_j = r_j(\mathbf{x}) = (0, \dots, \overset{j}{1}, \dots, 0, f_j^1, \dots, f_j^L) : j = 1, \dots, N\}$$

is a basis of the tangent space $T_{\mathbf{x}} \text{gr}(\mathbf{f})$ to $\text{gr}(\mathbf{f})$. Here $f_j^i = \partial_{x^j} f^i$. Let $\{e_i\}$ be an orthonormal frame of $T_{\mathbf{x}} \text{gr}(\mathbf{f})$. We have

$$e_i = B_i^j r_j$$

for some invertible matrix B_i^j .

Define the metric matrix for the basis $\{r_j\}$ by

$$g = (g_{kj}) \text{ with } g_{kj} = r_k \cdot r_j = \delta_{kj} + f_k^i f_j^i.$$

(We sum over i .) Then

$$\delta_{ij} = e_i \cdot e_j = B_i^k B_j^t r_k \cdot r_t = B_i^k B_j^t g_{kt} \Rightarrow I = (BB^T)g \Rightarrow BB^T = g^{-1}.$$

Thus BB^T is computable in terms of derivatives of \mathbf{f} .

Let $D_v w$ be the \mathbb{R}^{N+L} directional derivative of w in the direction v . Then

$$\begin{aligned} \text{Tr II} &= P^\nu D_{e_i} e_i = P^\nu D_{B_i^j r_j} B_i^k r_k = B_i^j P^\nu D_{r_j} B_i^k r_k \\ &= B_i^j P^\nu [(D_{r_j} B_i^k) r_k] + B_i^j B_i^k D_{r_j} r_k = B_i^j B_i^k P^\nu D_{r_j} r_k \\ &= (g^{-1})^{jk} P^\nu D_{r_j} r_k, \end{aligned}$$

since $P^\nu r_k = 0$.

We have

$$r_k = (0, \dots, 1, \dots, f_k^1(x^1, \dots, x^N), \dots, f_k^L(x^1, \dots, x^N)) = \partial_k^{\mathbb{R}^{N+L}} + \sum_{i=1}^L f_k^i \partial_{N+i}^{\mathbb{R}^{N+L}},$$

so in particular, $\partial_\ell^{\mathbb{R}^{N+L}} r_k = 0$ if $\ell > N$. Thus

$$D_{r_j} r_k = (0, \dots, \overset{N}{0}, f_{kj}^1, \dots, f_{kj}^L).$$

So far, we have

$$\text{Tr II} = (g^{-1})^{jk} P^\nu(0, \dots, 0, f_{kj}^1, \dots, f_{kj}^L).$$

Since g is given in terms of f , we need to write $P^\nu = I - P^T$ in terms of f . For any $v \in \mathbb{R}^{N+L}$, we have

$$\begin{aligned} P^T v &= (P^T v \cdot e_i) e_i = (v \cdot B_i^j r_j) B_i^k r_k = B_i^j B_i^k (v \cdot r_j) r_k \\ &= (g^{-1})^{jk} (v \cdot r_j) r_k. \end{aligned}$$

Thus

$$\begin{aligned} \text{Tr II} &= (g^{-1})^{jk} P^\nu(0, \dots, 0, f_{kj}^1, \dots, f_{kj}^L) \\ &= (g^{-1})^{jk} (0, \dots, 0, f_{kj}^1, \dots, f_{kj}^L) - P^T[(g^{-1})^{jk} (0, \dots, 0, f_{kj}^1, \dots, f_{kj}^L)] \\ &= (g^{-1})^{jk} (0, \dots, 0, f_{kj}^1, \dots, f_{kj}^L) - (g^{-1})^{jk} [(g^{-1})^{rs} (0, \dots, 0, f_{rs}^1, \dots, f_{rs}^L) \cdot r_j] r_k \\ &= (g^{-1})^{jk} (0, \dots, 0, f_{kj}^1, \dots, f_{kj}^L) - (g^{-1})^{jk} (g^{-1})^{rs} (f_{rs}^i f_j^i) r_k \\ &= (g^{-1})^{ij} \left(0, \dots, -(g^{-1})^{rs} f_{rs}^\ell f_i^\ell, \dots, 0, f_{ji}^1 - (g^{-1})^{rs} f_{rs}^\ell f_i^\ell f_j^1, \dots, f_{ji}^L - (g^{-1})^{rs} f_{rs}^\ell f_i^\ell f_j^L \right), \end{aligned} \tag{13}$$

after a relabeling of indices. Therefore, the last L component of Tr II are given by

$$\text{Tr II}^L = (g^{-1})^{ij} \left(f_{ji}^1 - (g^{-1})^{rs} f_{rs}^\ell f_i^\ell f_j^1, \dots, f_{ji}^L - (g^{-1})^{rs} f_{rs}^\ell f_i^\ell f_j^L \right).$$

C Proofs of the Steps for Theorem 2

C.1 Step 1

Lemma 3. (Step 1) $\lim_{\lambda \rightarrow 0} R_{D,P,\lambda}^* = 0$.

Proof. After the smoothing procedure in §3.1 for the distance penalty term, the function $R_{D,P,\lambda} : \mathcal{M} \rightarrow \mathbb{R}$ is continuous in the Fréchet topology on \mathcal{M} . We check that the functions $R_{D,P,\lambda} : \mathcal{M} \rightarrow \mathbb{R}$ are equicontinuous in λ : for fixed $\mathbf{f}_0 \in \mathcal{M}$ and $\epsilon > 0$, there exists $\delta = \delta(\mathbf{f}_0, \epsilon)$ such that $|\lambda - \lambda'| < \delta \Rightarrow |R_{D,P,\lambda}(\mathbf{f}_0) - R_{D,P,\lambda'}(\mathbf{f}_0)| < \epsilon$. This is immediate:

$$|R_{D,P,\lambda}(\mathbf{f}_0) - R_{D,P,\lambda'}(\mathbf{f}_0)| = |(\lambda - \lambda') \mathcal{P}_G(\mathbf{f}_0)| < \epsilon,$$

if $\delta < \epsilon / |\mathcal{P}_G(\mathbf{f}_0)|$. It is standard that the infimum $\inf R_\lambda$ of an equicontinuous family of functions is continuous in λ , so $\lim_{\lambda \rightarrow 0} R_{D,P,\lambda}^* = R_{D,P,\lambda=0}^* = R_{D,P}(\boldsymbol{\eta}) = 0$. \square

C.2 Step 2

We assume that the class probability function $\boldsymbol{\eta}(\mathbf{x}) : \mathbb{R}^N \rightarrow \mathbb{R}^L$ is smooth, and that the marginal distribution $\mu(\mathbf{x})$ is continuous. We also let μ denote the corresponding measure on \mathcal{X} .

Notation:

$$h_{\mathbf{f}}(\mathbf{x}) = \operatorname{argmax}\{f^\ell(\mathbf{x}), \ell \in \mathcal{Y}\}.$$

Of course,

$$\mathbb{1}_{h_{\mathbf{f}}(\mathbf{x}) \neq y} = \begin{cases} 1, & h_{\mathbf{f}}(\mathbf{x}) \neq y, \\ 0, & h_{\mathbf{f}}(\mathbf{x}) = y. \end{cases}$$

Lemma 4. (Step 2 for a subsequence)

$$\lim_{n \rightarrow \infty} R_{D,P}(\mathbf{f}_n) = 0 \Rightarrow \lim_{i \rightarrow \infty} R_P(\mathbf{f}_{n_i}) = R_P^*$$

for some subsequence $\{\mathbf{f}_{n_i}\}_{i=1}^\infty$ of $\{\mathbf{f}_n\}$.

Proof. The left hand side of the Lemma is

$$\int_{\mathcal{X}} d^2(\mathbf{f}_n(\mathbf{x}), \boldsymbol{\eta}(\mathbf{x})) d\mathbf{x} \rightarrow 0,$$

which is equivalent to

$$\int_{\mathcal{X}} d^2(\mathbf{f}_n(\mathbf{x}), \boldsymbol{\eta}(\mathbf{x})) \mu(\mathbf{x}) d\mathbf{x} \rightarrow 0, \quad (14)$$

since \mathcal{X} is compact and μ is continuous. Therefore, it suffices to show

$$\begin{aligned} \int_{\mathcal{X}} d^2(\mathbf{f}_n(\mathbf{x}), \boldsymbol{\eta}(\mathbf{x})) \mu(\mathbf{x}) d\mathbf{x} &\rightarrow 0 \\ \implies \mathbb{E}_P[\mathbb{1}_{h_{\mathbf{f}_n}(\mathbf{x}) \neq y}] &\rightarrow \mathbb{E}_P[\mathbb{1}_{h_{\boldsymbol{\eta}}(\mathbf{x}) \neq y}]. \end{aligned} \quad (15)$$

We recall that L^2 convergence implies pointwise convergence a.e, so (14) implies that a subsequence of \mathbf{f}_n , also denoted \mathbf{f}_n , has $\mathbf{f}_n \rightarrow \boldsymbol{\eta}(\mathbf{x})$ pointwise a.e. on \mathcal{X} . (By our assumption on $\mu(\mathbf{x})$, these statements hold for either μ or Lebesgue measure.) By Egorov's theorem, for any $\epsilon > 0$, there exists a set $B_\epsilon \subset \mathcal{X}$ with $\mu(B_\epsilon) < \epsilon$ such that $\mathbf{f}_n \rightarrow \boldsymbol{\eta}(\mathbf{x})$ uniformly on $\mathcal{X} \setminus B_\epsilon$.

Fix $\delta > 0$ and set

$$Z_\delta = \{\mathbf{x} \in \mathcal{X} : \#\{\operatorname{argmax}_{\ell \in \mathcal{Y}} \eta^\ell(\mathbf{x})\} = 1, |\max_{\ell \in \mathcal{Y}} \eta^\ell(\mathbf{x}) - \operatorname{submax}_{\ell \in \mathcal{Y}} \eta^\ell(\mathbf{x})| < \delta\},$$

where $\operatorname{submax}_{\ell \in \mathcal{Y}}$ denotes the second largest element in $\{\eta^1(\mathbf{x}), \dots, \eta^L(\mathbf{x})\}$. For the moment, assume that $Z_0 = \{\mathbf{x} \in \mathcal{X} : \#\{\operatorname{argmax}_{\ell \in \mathcal{Y}} \eta^\ell(\mathbf{x})\} > 1\}$ has $\mu(Z_0) = 0$.

It follows easily¹ that $\mu(Z_\delta) \rightarrow 0$ as $\delta \rightarrow 0$. On $\mathcal{X} \setminus (Z_\delta \cup B_\epsilon)$, we have $\mathbb{1}_{h_{\mathbf{f}_n}(\mathbf{x}) \neq y} = \mathbb{1}_{h_{\boldsymbol{\eta}}(\mathbf{x}) \neq y}$ for $n > N_\delta$. Thus

$$\mathbb{E}_P[\mathbb{1}_{\mathcal{X} \setminus (Z_\delta \cup B_\epsilon)} \mathbb{1}_{h_{\mathbf{f}_n}(\mathbf{x}) \neq y}] = \mathbb{E}_P[\mathbb{1}_{\mathcal{X} \setminus (Z_\delta \cup B_\epsilon)} \mathbb{1}_{h_{\boldsymbol{\eta}}(\mathbf{x}) \neq y}].$$

(Here $\mathbb{1}_A$ is the characteristic function of a set A .)

As $\delta \rightarrow 0$,

$$\mathbb{E}_P[\mathbb{1}_{\mathcal{X} \setminus (Z_\delta \cup B_\epsilon)} \mathbb{1}_{h_{\mathbf{f}_n}(\mathbf{x}) \neq y}] \rightarrow \mathbb{E}_P[\mathbb{1}_{\mathcal{X} \setminus B_\epsilon} \mathbb{1}_{h_{\mathbf{f}_n}(\mathbf{x}) \neq y}].$$

and similarly for \mathbf{f}_n replaced by $\boldsymbol{\eta}(\mathbf{x})$. During this process, N_δ presumably goes to ∞ , but that precisely means

$$\lim_{n \rightarrow \infty} \mathbb{E}_P[\mathbb{1}_{\mathcal{X} \setminus B_\epsilon} \mathbb{1}_{h_{\mathbf{f}_n}(\mathbf{x}) \neq y}] = \mathbb{E}_P[\mathbb{1}_{\mathcal{X} \setminus B_\epsilon} \mathbb{1}_{h_{\boldsymbol{\eta}}(\mathbf{x}) \neq y}].$$

Since

$$\left| \mathbb{E}_P[\mathbb{1}_{\mathcal{X} \setminus B_\epsilon} \mathbb{1}_{h_{\mathbf{f}_n}(\mathbf{x}) \neq y}] - \mathbb{E}_P[\mathbb{1}_{h_{\mathbf{f}_n}(\mathbf{x}) \neq y}] \right| < \epsilon,$$

and similarly for $\boldsymbol{\eta}(\mathbf{x})$, we get

$$\begin{aligned} &\left| \lim_{n \rightarrow \infty} \mathbb{E}_P[\mathbb{1}_{h_{\mathbf{f}_n}(\mathbf{x}) \neq y}] - \mathbb{E}_P[\mathbb{1}_{h_{\boldsymbol{\eta}}(\mathbf{x}) \neq y}] \right| \\ &\leq \left| \lim_{n \rightarrow \infty} \mathbb{E}_P[\mathbb{1}_{h_{\mathbf{f}_n}(\mathbf{x}) \neq y}] - \lim_{n \rightarrow \infty} \mathbb{E}_P[\mathbb{1}_{\mathcal{X} \setminus B_\epsilon} \mathbb{1}_{h_{\mathbf{f}_n}(\mathbf{x}) \neq y}] \right| \\ &\quad + \left| \lim_{n \rightarrow \infty} \mathbb{E}_P[\mathbb{1}_{\mathcal{X} \setminus B_\epsilon} \mathbb{1}_{h_{\mathbf{f}_n}(\mathbf{x}) \neq y}] - \mathbb{E}_P[\mathbb{1}_{\mathcal{X} \setminus B_\epsilon} \mathbb{1}_{h_{\boldsymbol{\eta}}(\mathbf{x}) \neq y}] \right| \\ &\quad + \left| \lim_{n \rightarrow \infty} \mathbb{E}_P[\mathbb{1}_{\mathcal{X} \setminus B_\epsilon} \mathbb{1}_{h_{\boldsymbol{\eta}}(\mathbf{x}) \neq y}] - \mathbb{E}_P[\mathbb{1}_{h_{\boldsymbol{\eta}}(\mathbf{x}) \neq y}] \right| \\ &\leq 3\epsilon. \end{aligned}$$

¹Let A_k be sets with $A_{k+1} \subset A_k$ and with $\mu(\cap_{k=1}^\infty A_k) = 0$. If $\mu(A_k) \not\rightarrow 0$, then there exists a subsequence, also called A_k , with $\mu(A_k) > K > 0$ for some K . We claim $\mu(\cap A_k) \geq K$, a contradiction. For the claim, let $Z = \cap A_k$. If $\mu(Z) \geq \mu(A_k)$ for all k , we are done. If not, since the A_k are nested, we can replace A_k by a set, also called A_k , of measure K and such that the new A_k are still nested. For the relabeled $Z = \cap A_k$, $Z \subset A_k$ for all k , and we may assume $\mu(Z) < K$. Thus there exists $Z' \subset A_1$ with $Z' \cap Z = \emptyset$ and $\mu(Z') > 0$. Since $\mu(A_i) = K$, we must have $A_i \cap Z' \neq \emptyset$ for all i . Thus $\cap A_i$ is strictly larger than Z , a contradiction. In summary, the claim must hold, so we get a contradiction to assuming $\mu(A_k) \not\rightarrow 0$.

(Strictly speaking, $\lim_{n \rightarrow \infty} \mathbb{E}_P[\mathbb{1}_{h_{f_n}(\mathbf{x}) \neq y}]$ is first lim sup and then lim inf to show that the limit exists.) Since ϵ is arbitrary, the proof is complete if $\mu(Z_0) = 0$.

If $\mu(Z_0) > 0$, we rerun the proof with \mathcal{X} replaced by Z_0 . As above, $f_n|_{Z_0}$ converges uniformly to $\eta(\mathbf{x})$ off a set of measure ϵ . The argument above, without the set Z_δ , gives

$$\int_{Z_0} \mathbb{1}_{h_{f_n}(\mathbf{x}) \neq y} \mu(\mathbf{x}) d\mathbf{x} \rightarrow \int_{Z_0} \mathbb{1}_{h_\eta(\mathbf{x}) \neq y} \mu(\mathbf{x}) d\mathbf{x}.$$

We then proceed with the proof above on $\mathcal{X} \setminus Z_0$. \square

Corollary 5. (Step 2 in general) For our algorithm, $\lim_{n \rightarrow \infty} R_{D,P}(f_{n,\lambda,m}) = 0 \Rightarrow \lim_{i \rightarrow \infty} R_P(f_{n,\lambda,m}) = R_P^*$.

Proof. Choose $f_{1,\lambda,m}$ as in Theorem 2. Since $V_{tot,\lambda,m}, f_{n,\lambda,m}$ has pointwise length going to zero as $n \rightarrow \infty$, $\{f_{n,\lambda,m}(\mathbf{x})\}$ is a Cauchy sequence for all \mathbf{x} . This implies that $f_{n,\lambda,m}$, and not just a subsequence, converges pointwise to η . \square

C.3 Step 3

Lemma 6. (Step 3) If $k \rightarrow \infty$ and $k/m \rightarrow 0$ as $m \rightarrow \infty$, then for $f \in \text{Maps}(\mathcal{X}, \Delta^{L-1})$,

$$|R_{D,\mathcal{T}_m}(f) - R_{D,P}(f)| \xrightarrow{m \rightarrow \infty} 0 \text{ in probability,}$$

for all distributions P that generate \mathcal{T}_m .

Proof. Since $R_{D,P}(f)$ is a constant for fixed f and P , convergence in probability will follow from weak convergence, i.e.,

$$\mathbb{E}_{\mathcal{T}_m}[|R_{D,\mathcal{T}_m}(f) - R_{D,P}(f)|] \xrightarrow{m \rightarrow \infty} 0.$$

We have

$$\begin{aligned} |R_{D,\mathcal{T}_m}(f) - R_{D,P}(f)| &= \left| \int_{\mathcal{X}} \left[d^2 \left(f(\mathbf{x}), \frac{1}{k} \sum_{i=1}^k \tilde{z}_i \right) - d^2(f(\mathbf{x}), \eta(\mathbf{x})) \right] d\mathbf{x} \right| \\ &\leq \int_{\mathcal{X}} \left| d^2 \left(f(\mathbf{x}), \frac{1}{k} \sum_{i=1}^k \tilde{z}_i \right) - d^2(f(\mathbf{x}), \eta(\mathbf{x})) \right| d\mathbf{x}. \end{aligned}$$

Set $\mathbf{a} = f(\mathbf{x}) - \frac{1}{k} \sum_{i=1}^k \tilde{z}_i$, $\mathbf{b} = f(\mathbf{x}) - \eta(\mathbf{x})$. Then

$$\begin{aligned} \left| \|\mathbf{a}\|_2^2 - \|\mathbf{b}\|_2^2 \right| &= \left| \sum_{\ell=1}^L a_\ell^2 - \sum_{\ell=1}^L b_\ell^2 \right| = \left| \sum_{\ell=1}^L (a_\ell^2 - b_\ell^2) \right| \\ &\leq \sum_{\ell=1}^L |a_\ell^2 - b_\ell^2| \leq 2 \sum_{\ell=1}^L |a_\ell - b_\ell| \max\{|a_\ell|, |b_\ell|\} \\ &\leq 2 \sum_{\ell=1}^L |a_\ell - b_\ell|, \end{aligned}$$

since $f^\ell(\mathbf{x}), \frac{1}{k} \sum_{i=1}^k \tilde{z}_i^\ell, \eta^\ell(\mathbf{x}) \in [0, 1]$. Therefore, it suffices to show that

$$\sum_{\ell=1}^L \mathbb{E}_{\mathcal{T}_m} \left[\int_{\mathcal{X}} \left| \left(f^\ell(\mathbf{x}) - \frac{1}{k} \sum_{i=1}^k \tilde{z}_i^\ell \right) - (f^\ell(\mathbf{x}) - \eta^\ell(\mathbf{x})) \right| d\mathbf{x} \right] \xrightarrow{m \rightarrow \infty} 0,$$

so the result follows if

$$\lim_{m \rightarrow \infty} \mathbb{E}_{\mathcal{T}_m, \mathbf{x}} \left[\left| \eta^\ell(\mathbf{x}) - \frac{1}{k} \sum_{i=1}^k \tilde{z}_i^\ell \right| \right] = 0 \text{ for all } \ell. \quad (16)$$

By Jensen's inequality $(\mathbb{E}[f])^2 \leq \mathbb{E}(f^2)$, (16) follows if

$$\lim_{m \rightarrow \infty} \mathbb{E}_{\mathcal{T}_m, \mathbf{x}} \left[\left(\eta^\ell(\mathbf{x}) - \frac{1}{k} \sum_i^k \tilde{z}_i^\ell \right)^2 \right] = 0 \text{ for all } \ell. \quad (17)$$

Let $\eta_{k,m}^\ell(\mathbf{x}) = \frac{1}{k} \sum_i^k \tilde{z}_i^\ell$. Then $\eta_{k,m}^\ell$ is actually an estimate of the class probability $\eta^\ell(\mathbf{x})$ by the k -Nearest Neighbor rule. Following the proof of Stone's Theorem [19, 9], if $k \xrightarrow{m \rightarrow \infty} \infty$ and $k/m \xrightarrow{m \rightarrow \infty} 0$, (17) holds for all distributions P . \square

D Additional Examples

While it is hard to plot the learned submanifold $\{(\mathbf{x}, \mathbf{f}(\mathbf{x}))\} \subset \mathbb{R}^2 \times \Delta^2$ for the three-class example given in Figure 1, we show in figure 4 another example of binary learning using our approach. In this example, the domain \mathcal{X} is still $2d$. Figure 4 shows the evolve of the estimated submanifold (where $\{(\mathbf{x}, \mathbf{f}(\mathbf{x}))\}$ becomes a surface in \mathbb{R}^3) and the corresponding decision boundary, which demonstrates the effect of our geometric regularization term in learning a volume minimizing submanifold to fit the training data. For this example, we implement a grid representation of \mathbf{f} , which is more faithful to our framework in Section 3, but not amenable for classification in high-dimensional input space (that is why we use a RBF-based parametric representation in Section 5). In particular, we initialize the domain of \mathbf{f} as a d^2 uniform grid and \mathbf{f} is approximated by its values on the grid point set.

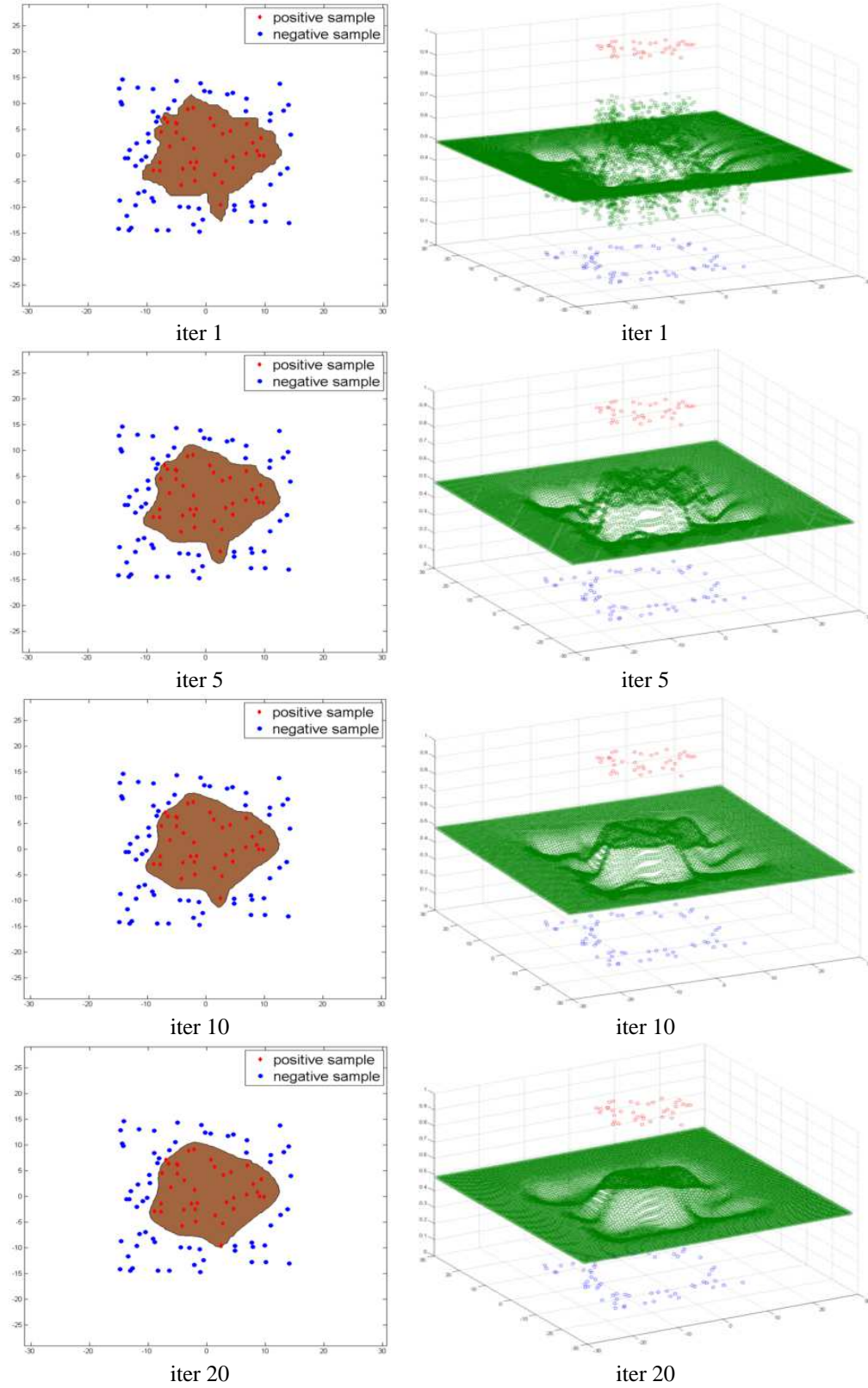


Figure 4: Example of binary learning, where input space \mathcal{X} is $2d$. Training points are sampled uniformly within the region $[-20, 20] \times [-20, 20]$, and labeled by the function $y = \text{sign}(10 - \|\mathbf{x}\|_2)$. We plot the evolve of the decision boundary obtained by our method in the left column, and the corresponding learned submanifold on the right column. Note that the vertical axis of the right image is the 1-simplex $\Delta^1 \subset \mathbb{R}^2$.